Synthetic aperture radar backscatter is influenced by bubbles at the ice/water interface of an Antarctic lake

Check for updates

Adam Gaudreau [1] ✉, Denis Lacelle [1] ✉ & Dale T. Andersen [2]

Synthetic aperture radar is an invaluable tool for monitoring lake ice. This study utilizes synthetic aperture radar to analyze the 2019-2023 backscatter time series of perennially ice-covered Lake Untersee in East Antarctica. We observed stark seasonal backscatter variations, averaging –9.6 dB from December to March and –3.7 dB from May to November. These fluctuations correspond to the abundance of sub-centimeter bubbles at the ice/water interface. Notably, the backscatter increase in April-May aligns closely with variations in ice thickness across the lake. Our findings suggest that ice cover thickness influences the timing and duration of ice accretion at the bottom, the accumulation of dissolved gases and bubbles, and the resultant changes in surface roughness at the ice/water interface. These factors collectively impact the backscatter response. This study enhances our understanding of the interactions between subsurface processes and synthetic aperture radar backscatter, shedding light on the seasonal dynamics of perennially ice-covered lakes.

The perennial ice-covers of Antarctic lakes are an important feature that influence the biogeochemistry of the water column and the benthic microbial ecosystem[1]. The thickness of perennial ice covers, typically in the 3–6 m range[2], is maintained by the equilibrium between water freezing onto the bottom of the ice cover and its ablation at the surface[3]. The water column of a perennially ice-covered lake (PICL) is often supersaturated in gases, with the saturation level mainly determined by the thickness of the ice cover and its effect on hydrostatic pressure. As water freezes to the bottom of the ice cover, the gases are exsolved, and the gas supersaturation level increases in the boundary layer[4–6]. Bubble nucleation begins when the total pressure of dissolved gases equals the local hydrostatic pressure at the ice/water interface. The gas bubbles then become included in the accreting ice and are eventually released into the atmosphere from the ablation of the ice cover[4,5]. The thickness and bubble content of the ice covers are thus critical to the benthic phototrophic ecosystem as they affect the optical properties (scattering and absorption caused by bubbles and sediments) of the ice cover and, therefore, the amount of light reaching the water column[7]. Therefore, knowledge about the spatial and temporal changes in internal optical properties of the perennial ice covers, including bubbles, in Antarctica is important to assess the state of the aquatic ecosystems and global environments.

Synthetic aperture radar (SAR) imagery is commonly used to infer lake ice conditions. Early studies recognized that variations in dissolved gas content in the water column may affect the formation of bubbles at the ice/water interface and impact backscatter intensities[8,9]. However, studies largely attributed the high backscatter over seasonally ice-covered lakes to the high dielectric contrast at the ice/water interface and a double bounce interaction between vertically oriented tubular bubbles within the ice[10]. Subsequent studies have used these scattering mechanisms to infer lake ice phenology (freeze-up and break-up) from changes in backscatter intensity time series from dense stacks of SAR imagery[11–15]. The grounding regimes of lake ice in winter were similarly inferred from abrupt drop-offs in the SAR backscatter time series because the lower dielectric contrast at an ice/sediment interface allows more energy to be transmitted into the lacustrine sediments rather than returning to the sensor[15–17]. Recently, it was found that bubbles at the ice/water interface of floating lake ice covers can produce the necessary roughness for high backscatter at C-band wavelengths, before tubular bubbles are included in the ice[18]. This discovery suggests that high backscatter can occur independently of a double-bounce mechanism from tubular bubbles within ice covers. Basin depth is considered as a limiting factor to dissolved gas buildup and bubble formation beneath lake ice covers[9,19]. Furthermore, previous research has indicated that the presence of bubbles within ice, influenced by dissolved gases, impacts SAR backscatter intensity[8,9]. It was also suggested that elevated dissolved N_2 levels in some Arctic lakes may lead to a denser distribution of bubbles within the ice during freezing and contribute to volumetric scattering and stronger

[1]Department of Geography Environment and Geomatics, University of Ottawa, 75 Laurier Ave. E, Ottawa, ON K1N 6N5, Canada. [2]Carl Sagan Center, SETI Institute, 339 Bernardo Ave, Suite 200 Mountain View, CA, USA. ✉e-mail: agaud097@uottawa.ca; dlacelle@uottawa.ca

backscatter intensities[20]. However, no field measurements were presented to confirm the presence of elevated N_2 or to characterize the properties of the ice covers and the presence of bubbles at the ice/water interface during the period of ice accretion. Thus, there are still outstanding questions regarding the spatial and temporal variability of dissolved gases and bubble abundance at the ice/water interface, and the effect on backscatter variability.

Studies investigating SAR backscatter of ice-covered lakes have been conducted only in the Arctic. Perennially ice-covered lakes in Antarctica are ideal candidates to further our understanding of the role of gas buildup and the development of bubbles at the ice/water interface on the seasonal SAR backscatter variability from lake ice. Antarctic PICLs have water columns that are supersaturated in gases and a floating ice cover containing a range of bubble morphologies[7,21,22], and their ice cover should be unaffected by ice phenology and grounding regimes. Here, we examine the spatio-temporal evolution of SAR backscatter over Lake Untersee, a large and deep PICL in central Queen Maud Land, East Antarctica[23] (Fig. 1). From a dense stack of Sentinel-1 C-band SAR imagery acquired between 2019 and 2023, combined with field measurements, we examine the potential relations between C-band SAR backscatter and bubbles at the ice/water interface. The backscatter intensities over Lake Untersee are compared with moat-forming PICLs from the McMurdo Dry Valleys (Antarctica), and Lake Hazen, a large seasonally ice-covered lake (SICL) in the Canadian high Arctic.

Results and Discussion
SAR Backscatter Intensity over Lake Untersee

The 2019-23 Sentinel-1 SAR record over Lake Untersee reveals two distinct periods during which backscatter intensities were predominantly low or high across the lake (Fig. 2). Each year, between December and March (austral summers), backscatter intensities over the entire lake were at their annual minima with an average of –9.6 and –8.4 dB in ascending and descending acquisitions, respectively. Conversely, backscatter intensities between May and November were at their annual maxima with an average of –3.7 and –2.9 dB in ascending and descending acquisitions, respectively. The small difference in backscatter intensity between trajectories (1.2 and 0.8 dB during minima and maxima, respectively) is likely due to the difference in viewing angle: the steeper off-nadir angles of the descending trajectory are more sensitive to surface roughness compared to the shallower off-nadir angles of ascending trajectory (i.e. ref. 11).

The shift from low to high backscatter intensities occurs in April/May and takes an average of 64 days to complete across Lake Untersee. Conversely, the shift from high to low intensities occurs between late November and early December and lasts on average only 20 days. However, at any given location on the lake, the switch in intensity occurs abruptly over a few days (Fig. 3). For example, between two consecutive ascending acquisitions on 16 and 22 November 2020, site BH03 recorded a sudden drop-off of 14.6 dB (from –2.9 to –17.5 dB), and between two consecutive ascending acquisitions on 27 April and 3 May 2021, site BH05 experienced an abrupt increase of 8.5 dB (from –13.2 to –4.6 dB).

The transitional phases show a spatio-temporal pattern of change across the lake (Fig. 2). The abrupt increase in intensity observed in April first occurs along the shorelines and gradually progresses toward the central region of the lake. The abrupt decreases in intensity observed in late November first occurred in the central regions and gradually progressed toward the shorelines. As such, the high backscatter period was the longest for regions along the shorelines, and the low backscatter period was longest for the central regions of the lake. An exception to this general concentric pattern of change in SAR intensity is the area on the southwestern side of the peninsula (Fig. 1). During each year of the SAR record, this region displayed low intensities for 1 or 2 months only (December and January) and experienced gradually increasing or high intensities for the rest of the year.

Several processes have been advanced to explain the abrupt and seasonal changes in backscatter intensity of SICLs in the Arctic. First, the seasonal changes in backscatter intensity are commonly associated with lake ice phenology. The onset of freezing and continued ice accretion during winter produces a high dielectric contract between ice and water, and the

occurrence of snow-ice layers, internal ice cracks and gas bubbles, deformation features, and ice/water interface roughness all introduce scattering surfaces that can produce high backscatter intensities. Conversely, the spring decay of an ice cover can produce both high intensities through the development of rough and irregular surface features, such as candle ice, and low intensities through the development of microwave-absorbent materials or smooth specular surfaces, like water-saturated snow or surface melt ponds[11,12,15]. Additionally, shallow SICLs can display sharp drop-offs in intensity if their thickening ice cover reaches the lakebed and grounds, leading to a decreased dielectric contrast between the coupled ice cover and lakebed sediments (e.g. ref. 14,15). Lake Untersee, on the other hand, has a perennial ice cover that does not give rise to a peripheral moat during the summer months. The thickness of the ice cover ranges between 2 and 4 meters, beneath which the water column extends down to a maximum reported depth of 169 meters. Surface water ponding on the ice is an uncommon and transient phenomenon at Lake Untersee. When it does occur, the prevailing winds coupled with the low humidity conditions in the area lead to its rapid removal by evaporation and sublimation. The sun cups that cover the ice surface throughout the year likely contribute to an increase in the overall backscatter intensity of the lake ice; however, their homogeneous physical properties across the lake cannot explain the observed seasonal changes in backscatter. Therefore, temporal changes in backscatter intensity associated with lake ice phenology, grounding of the ice cover, or sun cups at the ice surface can be ruled out.

Lower frequency microwave energy, including C-band, generally has a low sensitivity to snow, particularly dry and dense wind-compacted snow[24]. However, the Sentinel-1 imagery over Lake Untersee exhibited a high sensitivity to deep snow drifts. On 23 and 24 November 2021, 2–5 cm of snow fell over Lake Untersee. Most of the snow ablated within a few days, but some was redistributed into the north-west sector (Supplementary Note 1, Supplementary Fig. 1), creating wind-compacted snow drifts with thicknesses upwards of 30 to 40 cm with heavily wind-pitted surfaces, similar to the sun cups on the ice surface but on a smaller scale. Although the snow drifts increased backscatter over parts of the ice cover with values comparable to the high backscatter period (Supplementary Fig. 2), most of the snow in that area ablated within 1 to 3 weeks. Additionally, the patterns of snow redistribution across the lake are inconsistent with the concentric pattern of seasonal backscatter intensity change, and optical satellite imagery shows the ice cover to be largely free of snow between September and March (Supplementary Fig. 3). It is likely that the rough surface of the snow drifts temporarily increases backscatter, meaning that the presence of snow drifts can also be ruled out as a possible mechanism for the seasonal change in backscatter intensities. Therefore, the most accepted mechanisms proposed to explain backscatter intensity variability over Arctic SICLs do not apply to the observed seasonal variability of backscatter intensity for Lake Untersee.

Dynamic roughness at the ice/water interface drives seasonal changes in backscatter intensity

Surficial processes cannot explain the seasonal backscatter variations over Lake Untersee. This suggests that there must be a different mechanism(s) that enhances the seasonal scattering behaviour over Lake Untersee compared to SICLs. Based on ref. 18, we propose that gas bubbles at the ice/water interface of Lake Untersee can create enough roughness to produce a strong C-band backscatter response. This is consistent with 1) the recent discovery that single bounce at the ice/water interface is the dominant scattering mechanism for floating lake ice during a period when vertically oriented bubbles are also present in the ice cover[18,25], and 2) numerical modeling that suggests ice/water interface roughness is the most significant contribution to the backscatter response of floating lake ice[19,26]. Contrary to ref. 18 who considered bubbles at the ice/water interface to be static entities, our findings suggest that these bubbles, along with their associated radiometric roughness, exhibit spatial and seasonal variations. These variations are likely the primary drivers of the patterns in backscatter intensity observed over Lake Untersee.
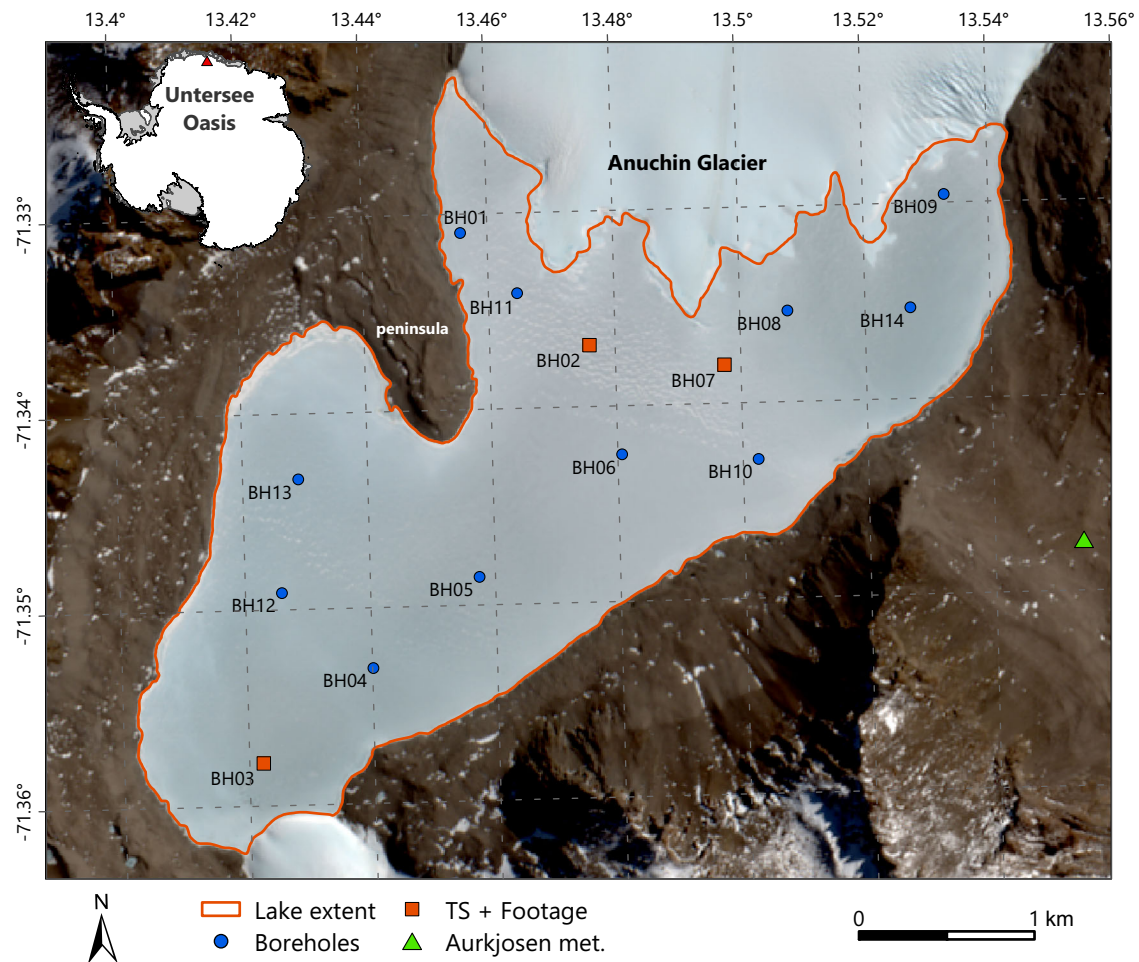
Fig. 1 | Lake Untersee, Dronning Maud Land, East Antarctica. Location map showing the Lake Untersee ice cover outline (orange line), the location of boreholes (BH) where water depth and ice thickness were measured (blue circle), the borehole locations used for backscatter time series analysis and where ice/water interface footage was captured (orange square), and the meteorological station in the Aurkjosen Valley just east of the lake (green triangle). The inset map shows the location of the Untersee Oasis relative to continent of Antarctica. Background is Sentinel-2 optical imagery acquired on 12 January 2018, courtesy of ESA Copernicus program. Map generated using ArcGIS Pro.

Lake Untersee's water column, like those in other Antarctic PICLs, demonstrates supersaturation with dissolved gases[4,5,27]. As gases exsolve from water freezing at the bottom of the ice cover and accumulate in the boundary layer, bubble nucleation can take place once the total pressure of dissolved gases exceeds that of the local hydrostatic pressure[4,6,28]. Dissolved oxygen (DO) profiles from Lake Untersee are here used to discern seasonal variations in gas saturation near the boundary layer. The DO saturation in Lake Untersee typically averages around 150 %, yet the profiles measured in mid-November to early December (Fig. 4) display notable differences compared to those measured in January and February. Specifically, the November/December profiles indicate that DO levels can rise by over 12 % at approximately 15 m depth relative to the deeper water, in contrast to the more uniform DO profiles observed in January and February that exhibit minimal variation throughout the water column[29,30]. This suggests that during the colder winter months, the exsolved gas from the water freezing process likely contributes to the observed increase in DO supersaturation beneath the ice cover, supporting more ice underside bubbles and enhancing scattering effects. Conversely, with reduced or absent ice formation during the warmer summer months, enhanced gas supersaturation in the boundary layer will likely integrate fully within the water column, supporting fewer interface bubbles and lowering backscatter. This mixing process, which unfolds over a monthly timescale, is further elaborated in ref. 31.

Video footage captured below the ice cover at three locations of Lake Untersee (BH02, BH03, and BH07) (Fig. 1) on or near the dates of SAR imagery acquisition was used to verify the presence of gas bubbles and their effect on backscatter intensity. In footage captured before 22 November 2022, gas bubbles were abundant under the ice cover at all three sites. The footage showed that a layer of densely packed bubbles completely covered the bottom of the ice within the field of view (Fig. 5). Conversely, in footage captured on and after 25 November 2022, the abundance of small gas bubbles under the ice at all three sites was substantially reduced. The lower abundance of bubbles also made it possible to observe that the bottom of the ice underside was smooth and had no large-scale undulations or pits. This characteristic can occur when the insulating effects of large gas bubbles and pockets limit ice accretion[32,33]. These observed changes in the abundance of bubbles match the abrupt decrease in backscatter intensity recorded at the three sites. Before 23 November 2022, the three sites had high backscatter intensities (−3.0, −1.4, and −2.5 dB for BH02, BH03, and BH07, respectively). However, on and after 24 November 2022, the three sites experienced a substantial decrease in backscatter intensity (−15.2, −7.6, and −7.0 dB for BH02, BH03, and BH07, respectively) and remained at these low values until March. These observations suggest that the abundance of bubbles at the ice/water interface affects the backscatter intensity over Lake Untersee.
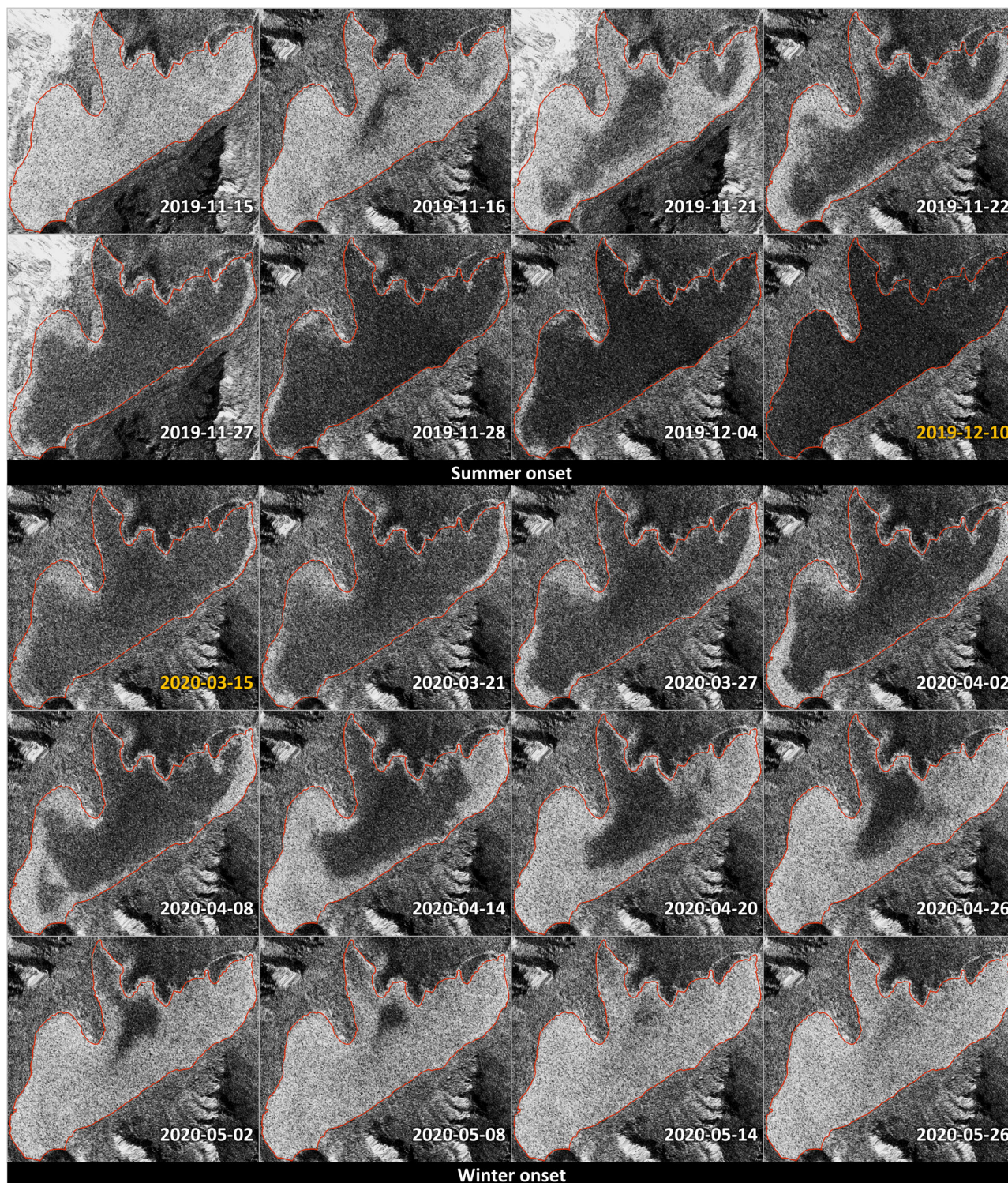
Fig. 2 | Patterns of backscatter change over the Lake Untersee ice cover. Examples of the spatio-temporal patterns of SAR backscatter intensity change that are regularly observed over Lake Untersee between seasons during the 4 years of available SAR imagery. Tiled imagery is Sentinel-1 SLC IW (courtesy of ESA Copernicus program) backscatter intensity as dB, processed and created using CATALYST Professional.

Ice/water interface bubble morphology and roughness

Bubbles at the ice/water interface of a floating lake ice cover can create the necessary roughness and produce high backscatter if the RMS height threshold of C-band wavelengths is exceeded (i.e. ref. [18]). Cores collected from the ice cover of Lake Untersee showed that it contains bubbles of various morphologies (spherical, oval, dendritic, and tubular), at times occupying as much as 50%vol[22]. Our footage also showed the presence of elongated tubular bubbles c. 10 to 100 cm in length distributed in the ice cover and revealed that bubbles were present in abundance at the ice/water interface during the period of high backscatter. Most of the bubbles at the interface were circular with a diameter of <1 cm, but many large gas pockets tens of centimeters to several meters in diameter were also present. Bubbles > 5 mm in diameter were flatter due to the large hydrostatic pressures that compress the gas against the ice. Although a range of bubble shapes was
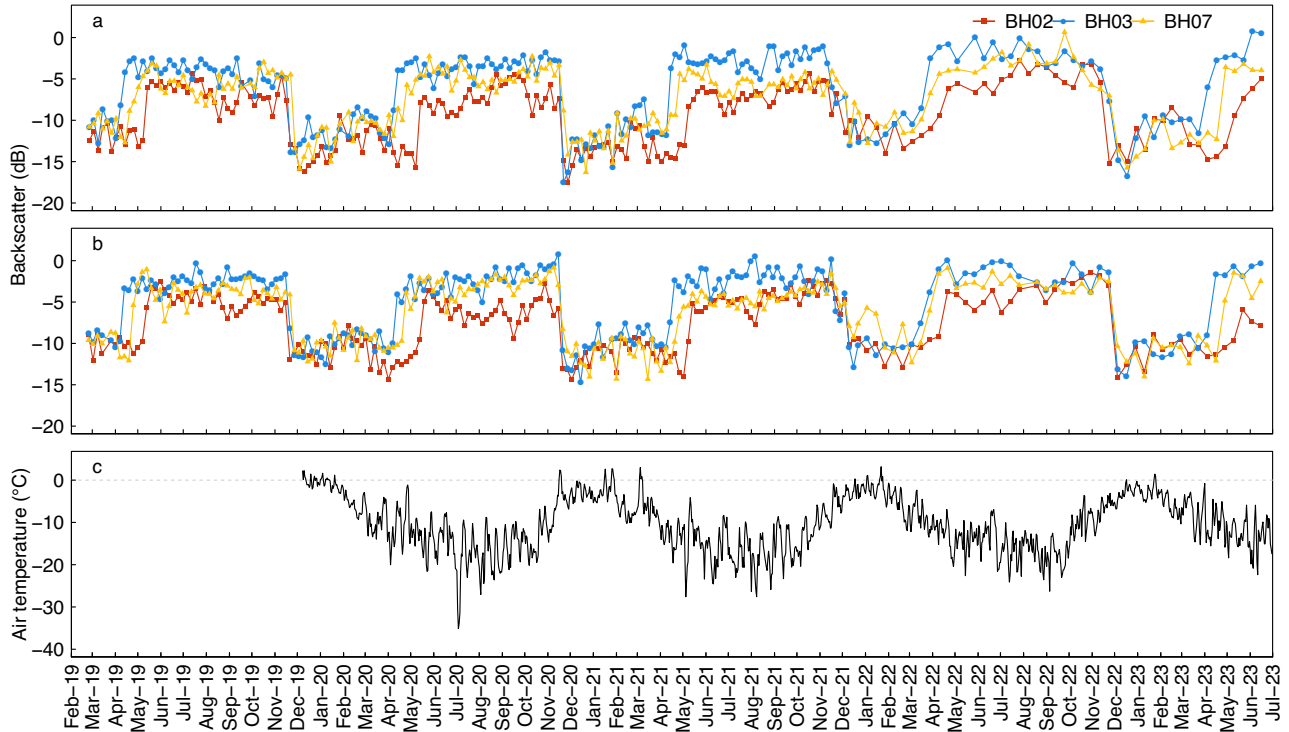
Fig. 3 | Time series of SAR backscatter and air temperature. Time series of SAR backscatter intensity as dB over BH02, BH03, and BH07 between February 2019 and July 2023 for **a** the ascending trajectory and **b** the descending trajectory. **c** The mean daily air temperature (°C) recorded between December 2019 and June 2023 by the Aurkjosen Valley meteorological station; dashed line is 0 °C.
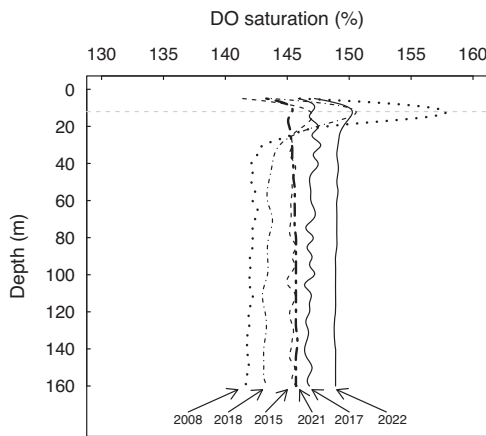
Fig. 4 | Dissolved oxygen profiles of the Lake Untersee water column. The saturation of dissolved oxygen in the lake basin was recorded annually between 2008 and 2022 in November/December. At this time of year, the saturation of dissolved oxygen is around 140-150 %, but can be elevated by c. 12 % near the surface, around 12 m depth (dashed horizontal line).

observed, all bubbles and gas pockets extended from the ice underside by <5 mm.

The bubbles that were observed at the ice/water interface satisfy the condition for surface roughness at C-band wavelengths according to the Fraunhofer criterion:

$$s < \frac{\lambda}{32 \cos \theta} \tag{1}$$

where surfaces with RMS height deviations less than s are considered smooth and specular with respect to the incident wavelength λ for a given

angle of incidence θ. Because this criterion assumes in situ wavelength, the sensor wavelength must be adjusted to account for to the relative permittivity ε' of the propagation material (ice):

$$\lambda = \frac{1}{\sqrt{\varepsilon'}} \frac{c}{f} \tag{2}$$

where c is the speed of light in a vacuum in m s^{-1} and f is the system frequency in Hz. We also account for the refracted angle of wave propagation following wave penetration into ice with Snell's law:

$$n_1 \sin \theta_1 = n_2 \sin \theta_2 \tag{3}$$

where n is the refractive index given with $\sqrt{\varepsilon'}$ and the subscripts 1 and 2 denote the media the wave travels from and to, respectively.

From these calculations, we obtain a shortened wavelength of 3.12 cm and shallower propagation angles of 19.8 and 17.3 ° for ascending and descending acquisitions, respectively, after penetrating pure ice with a $\varepsilon' = 3.17$. The actual average ε' for the Lake Untersee ice cover is closer to 3.09 due to its high bubble content, but this would not greatly affect the final wavelength. For Sentinel-1 with $f = 5.405$ GHz, we obtain a minimum RMS height threshold of c. 1.03 mm in both trajectories for the ice/water interface to be considered rough and capable of producing backward reflections. The dense and widespread coverage of bubbles at the ice/water interface with heights of c. 5 mm, such as those observed prior to 25 November, likely provide sufficient height variations to exceed the RMS height threshold. Therefore, it is likely that the relatively small bubbles <1 cm in diameter at the bottom of the ice cover of Lake Untersee are the dominant scattering source and their variable abundance provide the mechanism of the seasonal change in backscatter intensity. On the other hand, bubbles > 1 cm in diameter, gas pockets several meters in diameter, and the smooth ice surfaces, such as those observed on and after 25 November, would reduce backscatter as their relatively flat surfaces are akin to an interface of air and
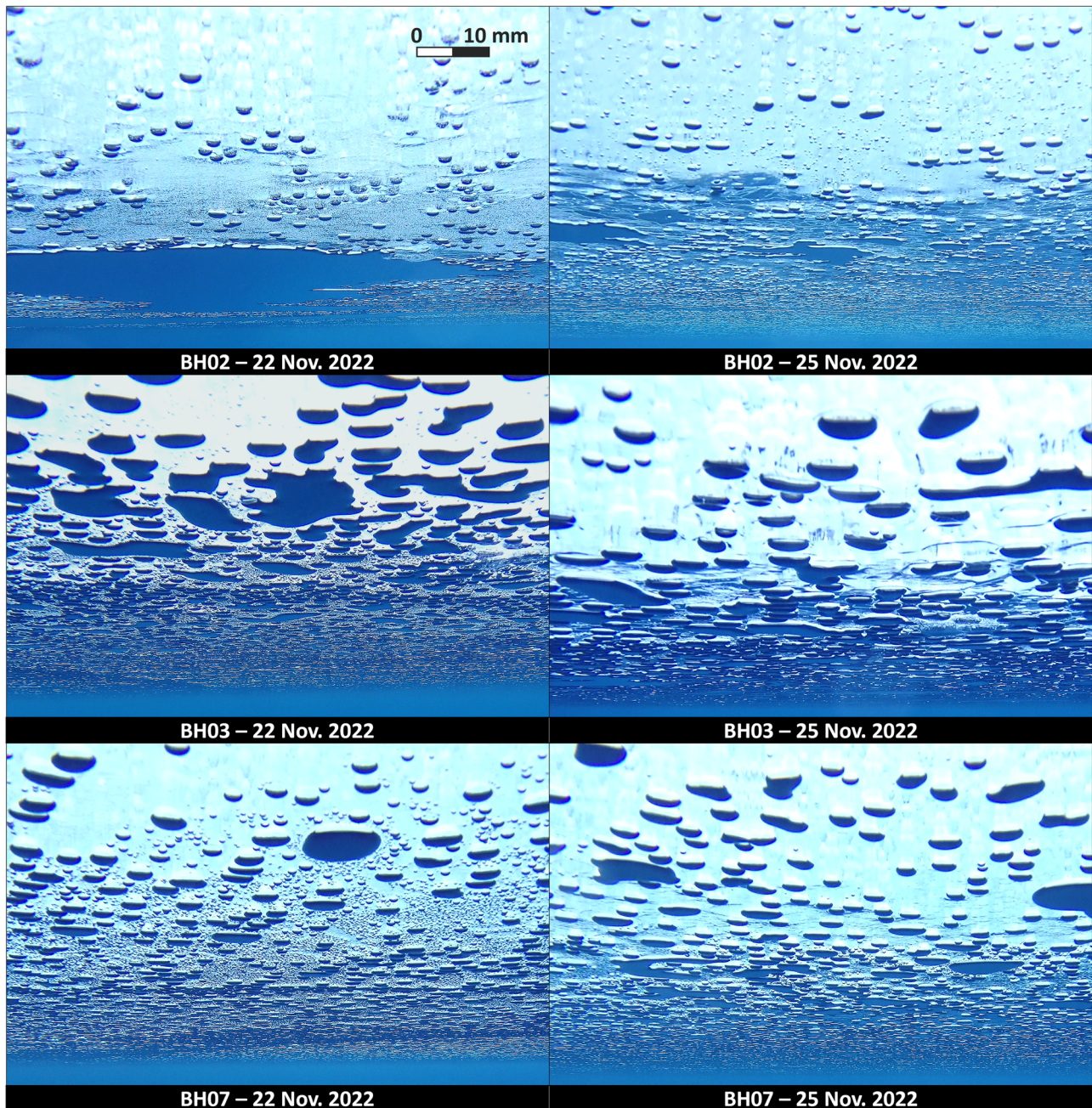
Fig. 5 | Bubbles under the Lake Untersee ice cover. Frames extracted from video footage captured under the ice cover at sites BH02, BH03, and BH7 on 22 and 25 November 2022. Note, the scale bar is only accurate for features at the top of the frames. Photos taken by AG using a submersible video camera attached to a rope.

calm water, reducing the RMS height deviations, leading to specular reflections away from the antenna.

Spatio-temporal variations in backscatter intensities over Lake Untersee

The nucleation and increased abundance of small gas bubbles at the ice/water interface would occur during the accretion period at the bottom of the ice cover. For PICLs, freezing takes place during the colder months when the temperature gradient through the ice cover is sufficiently strong to allow the latent heat of freezing to escape the ice cover and allow freezing to progress[3]. As a first-order estimate of the freezing period for Lake Untersee, we used the average daily air temperature between 2008 and 2023 to compute the thermal gradient through a 2.8 m thick ice cover and define the freezing period as the period when the average daily thermal gradient is below the average annual thermal gradient (Fig. 6). This approximation suggests that

freezing at the bottom of the ice cover takes place between April and November, which corresponds roughly to the timing of abrupt changes in backscatter intensities.

However, the onset and length of the freezing period at the ice/water interface should be lagged in relation to ice thickness (i.e. ref. [21]). From the SAR imagery, we observed that the switch from low to high intensities in April/May occurs earlier at places where the ice cover is thinner and up to 78 days later where the ice cover is thicker. In fact, the thickness of the ice cover is positively correlated with the average day-of-year (DOY) of the abrupt increase in backscatter intensity at the 14 boreholes during the 2019–2023 SAR record; Pearson's correlation coefficients are 0.87 ($p < 0.05$) and 0.82 ($p < 0.05$) for the ascending and descending trajectories, respectively (Fig. 7). This suggests that the ice thickness plays a key role in the timing of change from low to high intensities (i.e., ice thickness affects the onset of freezing and gas exsolution into the water and it sets the local hydrostatic pressure
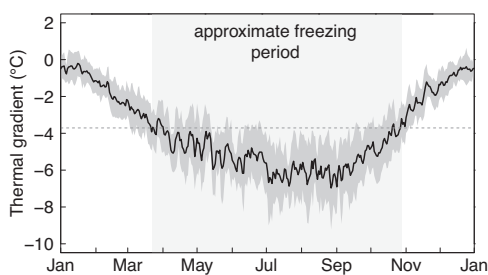
Fig. 6 | Approximate freezing period of the Lake Untersee ice cover. Average daily thermal gradient (black line) between surface air temperature and the ice/water interface (0 °C) for the Lake Untersee ice cover for an average ice thickness of 2.8 m between 2008 and 2023. The dark grey area is ±1 standard deviation, the dashed line is the average annual thermal gradient (−3.7 °C), and the light grey area is the approximate period when the daily gradient is below the all-time average gradient.
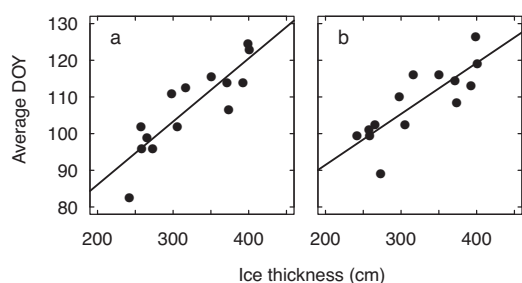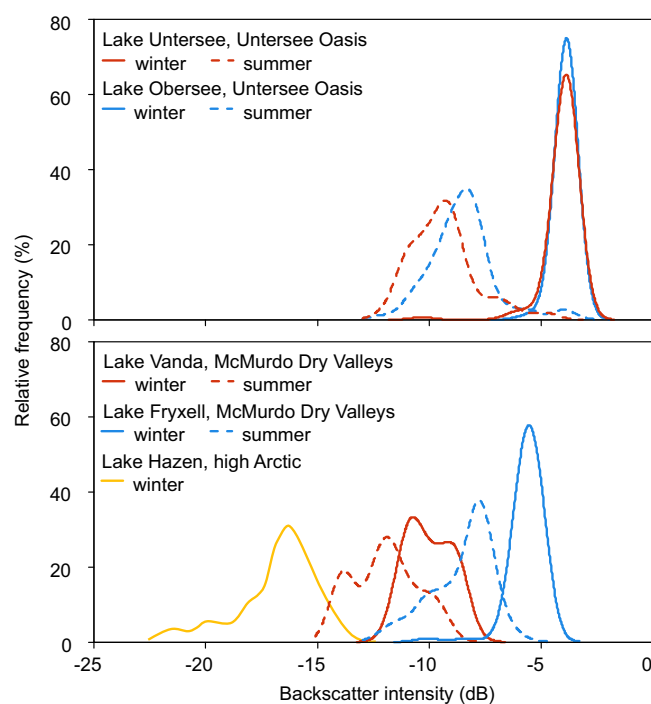

Fig. 7 | Relationship between the timing of backscatter change and ice thickness. Average day-of-year (DOY) of backscatter increase during the 4 years of SAR record at $n = 14$ boreholes as a function of ice thickness (cm) for **a** the ascending trajectory and **b** the descending trajectory. Black lines are the linear fit.


Fig. 8 | Relative frequency distribution of backscatter intensity over ice-covered lakes. Frequency distribution of Sentinel-1 backscatter intensity (as dB) between 2019 and 2023 over the entire ice cover of Lake Untersee, Lake Obersee, Lake Vanda, and Lake Fryxell during winter (April to October) and summer (November to March) and over Lake Hazen during winter (October to May).

which determines the timing of bubble nucleation and their abundance). However, no statistically significant correlation was found between the average DOY of the abrupt decrease in backscatter intensity and ice cover thickness, which lasts on average 20 days across the lake (Pearson's correlation coefficients of −0.32 ($p = 0.21$) and 0.30 ($p = 0.68$) in ascending and descending, respectively). The poor correlation could relate to the mixing of the exsolved gases under the ice cover in the water column following the end of the ice accretion period, a process that occurs independent of ice thickness and takes about one month to occur (i.e. ref. 31).

The area behind the peninsula has backscatter intensities that do not follow the trend observed for the rest of the lake. For example, despite having above-average ice thickness, the area behind the peninsula displays high backscatter intensities during much of the year (Fig. 2). Measurements of freeboard and ice thickness showed that the ice cover in this area has densities of 760 to 830 kg m^{-3}, while the rest of the ice cover has an average density of 902 kg m^{-3} [22]. An explanation for the under-dense ice behind the peninsula is its much higher bubble content. The area has the slowest circulation velocities because it is shielded by the peninsula[31]. The poor water circulation likely allows exsolved gases to remain in the boundary layer for longer and not mix with the water column below. This would promote more ice underside bubbles that become incorporated into the ice cover during freezing, ultimately reducing its density. More bubbles at the ice/water interface likely also explain the increased backscatter intensities in the area.

Comparison with other ice-covered lakes

Antarctica hosts numerous PICLs[1,2,34]. Here we compare the SAR backscatter intensities during the freezing period of Lake Untersee to three PICLs in Antarctica: Lake Obersee in the Untersee Oasis, and Lake Vanda and Lake Fryxell in the McMurdo Dry Valleys (MDV). We also compare to Lake Hazen, a large and deep SICL located in the Canadian high Arctic. Lake

Hazen was chosen because it is a large and deep lake, similar to Lake Untersee[35]. Sentinel-1 C-band SAR imagery was acquired and processed using the same methods as for Lake Untersee, and all comparisons here are made using the descending trajectory of Sentinel-1 (Supplementary Note 2).

The relative frequency distribution of winter backscatter intensities of the five lakes is shown in Fig. 8. Lake Untersee and Lake Obersee have similar average winter backscatter intensities (−3.7 and −3.6 dB, respectively). Conversely, Lake Vanda and Lake Fryxell have slightly lower winter backscatter intensities (−8.3 and −5.1 dB, respectively). We hypothesize that the differences between these four PICLs can be explained by the nature of their ice covers. Both Lake Untersee and Lake Obersee do not develop a summer moat, and as such their total dissolved gas pressure prior to the start of ice accretion is likely equal to the local hydrostatic pressure (Fig. 9a). This is reflected in their summer DO content (150 and 200 %, respectively), which is in equilibrium with the average thickness of their ice cover (3 and 4 m, respectively). Therefore, once the period of freezing begins, small bubbles can immediately form at the ice/water interface, increasing backscatter. Lake Vanda and Lake Fryxell, on the other hand, experience summer moating with open water along the shoreline that allows for partial degassing of the water column[5]. The lakes are also recharged in summer by glacial meltwater streams with air-saturated water (Fig. 9b)[36,37]. This reduces the summer DO content in the lakes (130–140 %), which is slightly lower than equilibrium with their ice cover thickness (3.5–4 and 4.5 m, respectively). In turn, this would lead to a delay in the nucleation of bubbles when freezing begins since the total gas content must first reach and exceed the local hydrostatic pressure for bubbles to form. As a result, there might be a lower abundance of small bubbles at the ice/water interface of moat-forming PICLs compared to the Untersee Oasis lakes, explaining their lower backscatter intensity.

The relative frequency distribution of winter backscatter intensity for Lake Hazen reveals a prominent peak at −15.9 dB (Fig. 8). This intensity is similar to other deep SICLs, such as Tazlina Lake (i.e. ref. 14), but is c. 10-12 dB lower than PICLs. We hypothesize that SICLs have substantially lower winter
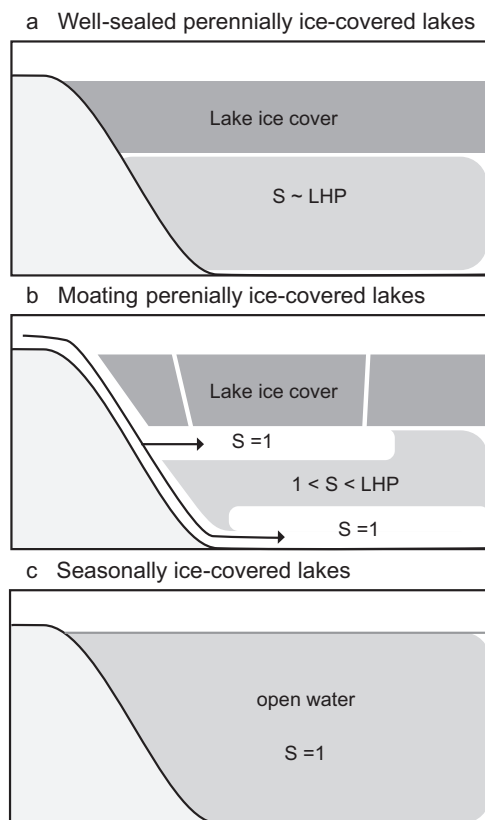
Fig. 9 | Diagram of lake gas saturation between different lake ice cover types prior to freezing. a Well-sealed perennially ice-covered lakes maintain a supersaturated water column with dissolved gas saturation (S) near the local hydrostatic pressure (LHP) of the ice cover. **b** Moat forming perennially ice-covered lakes have air-saturated inputs from glacial meltwater, diluting or stratifying the supersaturated water column. **c** The ice-off period of seasonally ice-covered lakes allows the water column S to reach equilibrium with the atmosphere through mixing and degassing. The figure is expanded from ref. 4.

backscatter intensities because they lose their ice cover during the summer, which causes the total dissolved gas content to reach equilibrium with atmospheric conditions (Fig. 9c). When the ice starts to develop in Arctic lakes, bubbles at the ice/water interface will not form until the total dissolved gas pressure exceeds the local hydrostatic pressure of the growing ice cover. This lag can be further amplified by the weight of surface snow, increasing the hydrostatic pressure, and by the mixing of dissolved gases within the reservoir, a process influenced by basin depth and mixing dynamics[9,14,19]. Consequently, it is evident that the SAR backscatter intensity of PICLs is more sensitive to the presence of small bubbles at the ice/water interface, which increase surface roughness. The total dissolved gas content in PICLs prior to ice accretion already approaches the local hydrostatic pressure, facilitating rapid bubble nucleation once freezing commences. This is not the case for SICLs.

Implications for future studies

To the best of our knowledge, this is the first study to investigate changes in SAR backscatter intensity over PICLs in Antarctica. At Lake Untersee, abrupt seasonal changes in backscatter intensity between 2019 and 2023 likely relate to the abundance of small bubbles at the ice/water interface, which is correlated with variations in ice thickness. These variations in ice thickness across the lake, in turn, set the local hydrostatic pressure and affect the seasonal rates of freezing and gas rejection at the ice/water interface, the timing of bubble nucleation, bubble abundance, and ultimately roughness and backscatter intensity. The seasonal build-up of dissolved gas during freezing at the ice/water interface is corroborated by the comparison with other PICLs in Antarctica; several MDV lakes are known to have seasonal gas budgets similar to Lake Untersee and display similar backscatter

phenomena. As such, PICLs are good candidates for studying the effects of gases at the ice/water interface on SAR backscatter from floating lake ice. Consequently, more consideration should be given to the effects of dissolved gas buildup and bubble formation at the ice/water interface during the interpretation of SAR backscatter from lake ice. Additionally, future work should also consider the temporal and spatial evolution of ice/water interface RMS height threshold for radiative transfer model parameterization (i.e. ref. 19).

Our findings from a well-sealed PICL may also be applicable as an analogue for the Europa Clipper mission. Europa, one of Jupiter's icy moons, is believed to harbour a liquid ocean beneath its icy crust. The REASON instrument (a radar profiler) aboard the Europa Clipper could collect critical information about the dynamics of gas buildup and bubble formation below Europa's floating icy crust. This could be crucial for understanding the internal structure of floating ice and advancing the search for extraterrestrial life.

Methods

Study site

Lake Untersee (71.34 ° S, 13.47° E) is located c. 612 m above sea level (asl) in the Gruber Mountains of East Antarctica (Fig. 1). The 2008-19 mean annual air temperature and relative humidity at Lake Untersee is −9.5 °C ± 0.7 °C and 42 ± 5 %, respectively[22,38]. Despite having a relatively warm mean annual air temperature for Antarctica, the climate is dominated by intense sublimation that limits surface melting due to cooling associated with the latent heat of sublimation[39,40]. The average wind speed is 5.4 m s^{-1} and is dominated by persistent southerlies that descend from the glaciers in the south and sweep across the lake[38].

Lake Untersee has a surface area of 11.4 km^2 and a volume of 5.21 × 10^8 m$^{3 \, 41}$. The ice cover has an average thickness of 2.77 m (ranges between 1.96 and 3.96 m), with the thinnest ice cover found in areas exposed to persistent winds that enhance sublimation[22]. The ice cover of Lake Untersee is in steady state because ice thickness measurements from the same location showed little variation over 6 years (± 0.07 m). This indicates that the freezing and ablation rates of the ice cover are nearly equal (i.e. ref. 3). Measurements from ablation ropes provided rates of 40 ± 1.2 cm yr.$^{-1}$ and 75 ± 4.2 cm yr.$^{-1}$ in the northern and southern sectors, respectively, which are comparable to freezing rates estimated from δ^{18}O profiles in the ice cover[22]. The entire surface of the ice cover remains rough year-round with sun cups c. 5 cm in depth and c. 10 cm wide, formed through a combination of sublimation and wind erosion. The ice cover contains bubbles of various morphologies (spherical, oval, dendritic, and tubular), sometimes occupying as much as 50 %vol[22]. The bubbles span a range of lengths and diameters, commonly exceeding 1 m in length and 1 cm in diameter. Summer heating promotes the formation of Tyndall figures in the near-surface of the ice cover resulting in whiter-appearing ice with increased optical scattering[7].

The lake is glacially dammed at its northern sector by the Anuchin Glacier and is recharged by subaqueous melting of the glacier and a subglacial meltwater source[22]. The lake has two sub-basins: a large northern oxic basin reaching a maximum depth of 169 m and a smaller southern basin with a maximum depth of 100 m. The water becomes anoxic below the depth of a dividing sill around 60 m. The oxic water is well mixed on a monthly timescale[31] and is supersaturated in gases with dissolved oxygen (DO) reaching 145-150 % in austral summer, a value consistent with the hydrostatic pressure caused by the ice cover[29,30,42,43]. Gas bubbles are commonly observed at the ice/water interface, ranging from a few millimeters to meters in diameter. Occasionally, drilling through the ice cover into large gas pockets produces geysers that erupt for several days.

SAR imagery and processing

Sentinel-1 interferometric wide swath single-look complex imagery over Lake Untersee between February 2019 and June 2023, inclusively, was obtained from the European Space Agency (ESA). Both ascending and

descending orbit directions were available in single horizontal co-polarization (HH) giving a 4-year SAR record with a total of 435 acquisitions. The pixel spacing is 14.1 m in track and 3.85 m in range for both trajectories, and the angle of incidence for the center and extent of the lake is 36.7 (range of 36.6 to 36.8) and 31.5 (range of 31.4 to 31.6) degrees for ascending and descending trajectories, respectively.

PCI Geomatics CATALYST Professional software was used for SAR imagery processing. The steps included radiometric calibration to sigma naught quantities, co-registration to one common reference image, multi-looking (1×4 in track and range, respectively) to reduce speckle and give roughly square pixels, and orthorectification to WGS 84 UTM Zone 33 D (south) using the global 30-m cell size (GLO-30; ESA Copernicus product) digital elevation model. The processed imagery was then used to analyze patterns of backscatter intensity over the lake and to produce time series of backscatter intensity for select locations (Fig. 1). For the time series analysis, pixel intensities over an area of 3×3 pixels (c. 42×42 m) around the select locations were averaged to smooth large variations in pixel values and converted to the decibel (dB) scale.

Field measurements

The meteorological station along the shoreline of Lake Untersee (612 m asl) was damaged following a glacial outburst flood in January 2019[41] and a new station was installed in the nearby Aurkjosen Valley (625 m asl). The 2019-22 mean daily air temperature from the Aurkjosen Valley station was compared with the time series of backscatter intensity to infer the ice cover freezing period.

In November 2022, water depth and ice cover thickness were measured at 14 sites across the lake (Fig. 1; Supplementary Table 1). Three boreholes were then selected to compare the SAR backscatter time series with observations of the presence and morphology of gas bubbles under the ice cover close to or on the day of scheduled Sentinel-1 flyovers in November-December 2022. Sites BH02 and BH03 were selected because they corresponded with areas of thick ice (4 m) and thin ice (2.5 m), respectively, and site BH07 was selected as a region of interest during preliminary SAR analysis and had a relatively thick ice cover (3.7 m). The observations under the ice cover were made with a video camera recording 4 K, 30 frames per second. All footage was captured with the same viewing angle using a camera rigging apparatus lowered down the borehole. Individual frames were then extracted from the footage when the camera was just below the ice cover looking up at the ice/water interface.

Data availability

Figures 2, 3, and 8 were made using open-source Sentinel-1 imagery. The full Sentinel-1 dataset used in this study is accessible free of charge through the European Space Agency (ESA) Copernicus program. The data can be obtained from the Copernicus Open Access Hub [https://scihub.copernicus.eu/] and from the Alaska Satellite Facility (ASF) Vertex web platform [https://asf.alaska.edu/] Source data for Fig. 5: [https://osf.io/dgh6m/?view_only=bfcbf54991e847d2b394677681a27091].

References

1. Vincent, W. & Laybourn-Parry, J. *Polar Lakes and Rivers: Limnology of Arctic and Antarctic Aquatic Ecosystems*. (Oxford University Press, 2008).
2. Priscu, J. C. et al. Perennial Antarctic lake ice: an oasis for life in a polar desert. *Science (1979)* **280**, 5372 (1998).
3. McKay, C. P., Clow, G. D., Wharton, R. A. Jr & Squyres, S. W. Thickness of ice on perennially frozen lakes. *Nature* **313**, 561–562 (1985).
4. Andersen, D. T., McKay, C. P. & Wharton, R. A. Dissolved gases in perennially ice-covered lakes of the McMurdo Dry Valleys, Antarctica. *Antarct Sci* **0**, 124–133 (1998).
5. Craig, H., Wharton, R. A. & McKay, C. P. Oxygen Supersaturation in Ice-Covered Antarctic Lakes: Biological Versus Physical Contributions. *Science (1979)* **255**, 318–321 (1992).
6. Lipp, G., Körber, C. H., Englich, S., Hartmann, U. & Rau, G. Investigation of the Behavior of Dissolved Gases during Freezing. *Cryobiology* **24**, 489–503 (1987).
7. McKay, C. P., Clow, G. D., Andersen, D. T. & Wharton, R. A. Light transmission and reflection in perennially ice-covered Lake Hoare, Antarctica. *J. Geophys. Res.* **99**, 20427–20444 (1994).
8. Jeffries, M. O., Morris, K., Weeks, W. F. & Wakabayashi, H. Structural and stratigraphic features and ERS 1 synthetic aperture radar backscatter characteristics of ice growing on shallow lakes in NW Alaska, winter 1991-1992. *J. Geophys. Res.* **99**, 22459–22471 (1994).
9. Mellor, J. C. Bathymetry of Alaskan Arctic Lakes: a key to resource inventory with remote-sensing methods. (1982).
10. Weeks, W. F., Fountain, A. G., Bryan, M. L. & Elachi, C. Differences in radar return from ice-covered North Slope Lakes. *J Geophys. Res.* **83**, 4069–4073 (1978).
11. Duguay, C. R., Pultz, T. J., Lafleur, P. M. & Drai, D. RADARSAT backscatter characteristics of ice growing on shallow sub-Arctic lakes, Churchill, Manitoba, Canada. *Hydrol. Process* **16**, 1631–1644 (2002).
12. Murfitt, J. & Duguay, C. R. Assessing the Performance of Methods for Monitoring Ice Phenology of the World's Largest High Arctic Lake Using High-Density Time Series Analysis of Sentinel-1 Data. *Remote Sens. (Basel)* **12**, 1–25 (2020).
13. Surdu, C. M., Duguay, C. R., Pour, H. K. & Brown, L. C. Ice freeze-up and break-up detection of shallow lakes in Northern Alaska with spaceborne SAR. *Remote Sens. (Basel)* **7**, 6133–6159 (2015).
14. Morris, K., Jeffries, M. O. & Weeks, W. F. Ice processes and growth history on Arctic and sub-Arctic lakes using ERS-1 SAR data. *Polar Record.* **31**, 115–128 (1995).
15. Antonova, S. et al. Monitoring Bedfast Ice and Ice Phenology in Lakes of the Lena River Delta Using TerraSAR-X Backscatter and Coherence Time Series. *Remote Sens. (Basel)* **8**, 903 (2016).
16. Engram, M., Arp, C. D., Jones, B. M., Ajadi, O. A. & Meyer, F. J. Analyzing floating and bedfast lake ice regimes across Arctic Alaska using 25 years of space-borne SAR imagery. *Remote Sens. Environ.* **209**, 660–676 (2018).
17. Jeffries, M. O., Wakabayashi, H. & Weeks, W. F. ERS-1 SAR backscatter changes associated with ice growing on shallow lakes in arctic Alaska. in *International Geoscience and Remote Sensing Symposium (IGARSS)* vol. 4 2001–2004 (Publ by IEEE, 1993).
18. Gunn, G. E., Duguay, C. R., Atwood, D. K., King, J. & Toose, P. Observing Scattering Mechanisms of Bubbled Freshwater Lake Ice Using Polarimetric RADARSAT-2 (C-Band) and UW-Scat (X- A nd Ku-Bands). *IEEE Trans. Geosci. Remote Sens.* **56**, 2887–2903 (2018).
19. Murfitt, J., Duguay, C., Picard, G. & Gunn, G. Forward modelling of synthetic aperture radar backscatter from lake ice over Canadian Subarctic Lakes. *Remote Sens. Environ.* **286**, 113424 (2023).
20. Dabboor, M. & Shokr, M. Sensitivity of Compact Polarimetric SAR Parameters to Modeled Lake Ice Growth. *IEEE Trans. Geosci. Remote Sens.* **59**, 9953–9967 (2021).
21. Adams, E. E., Priscu, J. C., Fritsen, C. H., Smith, S. R. & Brackman, S. L. Permanent Ice Covers of the McMurdo Dry Valley Lakes, Antarctica: Bubble Formation and Metamorphism. in *Ecosystem Dynamics in a Polar Desert: the Mcmurdo Dry Valleys, Antarctica* vol. 72 281–295 (1998).
22. Faucher, B., Lacelle, D., Fisher, D. A., Andersen, D. T. & McKay, C. P. Energy and water mass balance of Lake Untersee and its perennial ice cover, East Antarctica. *Antarct. Sci.* **31**, 271–285 (2019).
23. Hermichen, W.-D., Kowski, P. & Wand, U. Lake Untersee, a first isotope study of the largest freshwater lake in the interior of East Antarctica. *Nature* **315**, 131–133 (1985).

24. King, J. M. L. et al. UW-Scat: A Ground-Based Dual-Frequency Scatterometer for Observation of Snow Properties. *IEEE Geosci Remote Sens Lett* **10**, 528–532 (2013).

25. Atwood, D. K. et al. Microwave Backscatter from Arctic Lake Ice and Polarimetric Implications. *IEEE Trans. Geosci. Remote Sens* **53**, 5972–5982 (2015).

26. Murfitt, J., Duguay, C. R., Picard, G. & Gunn, G. E. Investigating the Effect of Lake Ice Properties on Multifrequency Backscatter Using the Snow Microwave Radiative Transfer Model. *IEEE Trans. Geosci. Remote Sens* **60**, 1–23 (2022).

27. Wharton, R. A., McKay, C. P., Mancinelli, R. L. & Simmons, G. M. Perennial N2 supersaturation in an Antarctic lake. *Nature* **325**, 343–345 (1987).

28. Yoshimura, K., Inada, T. & Koyama, S. Growth of spherical and cylindrical oxygen bubbles at an ice-water interface. *Cryst. Growth Des.* **8**, 2108–2115 (2008).

29. Wand, U., Schwarz, G., Brüggemann, E. & Bräuer, K. Evidence for physical and chemical stratification in lake untersee (central Dronning Maud Land, East Antarctica). *Antarct. Sci.* **9**, 43–45 (1997).

30. Wand, U., Samarkin, V. A., Nitzsche, H.-M. & Hubberten, H.-W. Biogeochemistry of methane in the permanently ice-covered Lake Untersee, central Dronning Maud Land, East Antarctica. *Limnol. Oceanogr.* **51**, 1180–1194 (2006).

31. Steel, H. C. B., McKay, C. P. & Andersen, D. T. Modeling circulation and seasonal fluctuations in perennially ice-covered and ice-walled lake untersee, antarctica. *Limnol. Oceanogr.* **60**, 1139–1155 (2015).

32. Engram, M., Anthony, K. W., Meyer, F. J. & Grosse, G. Synthetic aperture radar (SAR) backscatter response from methane ebullition bubbles trapped by thermokarst lake ice. *Canadian J. Remote Sens* **38**, 667–682 (2012).

33. Engram, M., Anthony, K. W., Meyer, F. J. & Grosse, G. Characterization of L-band synthetic aperture radar (SAR) backscatter from floating and grounded thermokarst lake ice in Arctic Alaska. *Cryosphere* **7**, 1741–1752 (2013).

34. Doran, P. T. et al. Paleolimnology of Extreme Cold Terrestrial and Extraterrestrial Environments. in *Long-term Environmental Change in Arctic and Antarctic Lakes* (eds. Pienitz, R., Douglas, M. S. V. & Smol, J. P.) vol. 8 578 (Springer, 2007).

35. Lehnherr, I. et al. The world's largest High Arctic lake responds rapidly to climate warming. *Nat. Commun.* **9**, 1290 (2018).

36. Schutte, C. A. et al. Vertical stratification and stability of biogeochemical processes in the deep saline waters of Lake Vanda, Antarctica. *Limnol. Oceanogr.* **65**, 569–581 (2020).

37. Hood, E. M., Howes, B. L. & Jenkins, W. J. Dissolved gas dynamics in perennially ice-covered Lake Fryxell, Antarctica. *Limnol. Oceanogr.* **43**, 265–272 (1998).

38. Andersen, D. T., McKay, C. P. & Lagun, V. Climate Conditions at Perennially Ice-Covered Lake Untersee, East Antarctica. *J. Appl. Meteorol. Climatol.* **54**, 1393–1412 (2015).

39. Hoffman, M. J., Fountain, A. G. & Liston, G. E. Surface energy balance and melt thresholds over 11 years at Taylor Glacier, Antarctica. *J. Geophys. Res. Earth Surf.* **113**, 1–12 (2008).

40. van den Broeke, M., van de Berg, W., van Meijgaard, E. & Reijmer, C. Identification of Antarctic ablation areas using a regional atmospheric climate model. *J. Geophys. Res. Atmosph.* **111**, 1–14 (2006).

41. Faucher, B. et al. Glacial lake outburst floods enhance benthic microbial productivity in perennially ice-covered Lake Untersee (East Antarctica). *Commun. Earth Environ.* **2**, 1–12 (2021).

42. Andersen, D. T., Sumner, D. Y., Hawes, I., Webster-Brown, J. & McKay, C. P. Discovery of large conical stromatolites in Lake Untersee, Antarctica. *Geobiology* **9**, 280–293 (2011).

43. Marsh, N. B. et al. Sources of solutes and carbon cycling in perennially ice-covered Lake Untersee, Antarctica. *Sci. Rep.* **10**, 1–12 (2020).

Author contributions

A.G.: study design and lead researcher, collected field data, acquired and processed SAR data, performed data manipulations and analyses. D.L.: contributed to data and results interpretation. D.A.: contributed to data and results interpretation. All authors contributed to manuscript editing.

Competing interests

The authors declare no competing interests.

Additional information

Supplementary information The online version contains supplementary material available at https://doi.org/10.1038/s43247-024-01370-2.

Correspondence and requests for materials should be addressed to Adam Gaudreau or Denis Lacelle.

Peer review information *Communications Earth & Environment* thanks the anonymous reviewers for their contribution to the peer review of this work. Primary Handling Editors: Kerstin Schepanski and Clare Davis. A peer review file is available.

Reprints and permissions information is available at http://www.nature.com/reprints

Publisher's note Springer Nature remains neutral with regard to jurisdictional claims in published maps and institutional affiliations.